Rheologica Acta
https://doi.org/10.1007/s00397-026-01556-9

ORIGINAL CONTRIBUTION

Multi-variable implicit viscosity model for shear-thinning fluids

Mohammad Amin Ghorbani[1,2] · Mohammad Pourhosseinian[2,3] · Florian Arthofer[4] · Silke Koch[4] · Christian Marschik[3] · Daniela Misul[5] · Bahram Haddadi[3]

Received: 9 December 2025 / Revised: 5 February 2026 / Accepted: 22 February 2026

Abstract
Accurately modeling the viscosity of shear-thinning elastomer compounds is crucial for optimizing their performance in industrial applications. Classical models (Power Law, Carreau, Cross) cannot directly account for temperature, and when coupled with temperature models (Arrhenius, WLF, VTF), they become mathematically complex and computationally costly for simulations. This study introduces the Multi-Variable Implicit (MVI) viscosity model, derived using machine learning-based symbolic regression. It offers a simplified mathematical structure while maintaining high predictive accuracy. The MVI model implicitly incorporates both shear-rate and temperature dependence in a single expression, while also capturing zero-shear viscosity through a Newtonian plateau. This feature ensures numerical stability and yields physically meaningful results across a wide range of shear rates and temperatures. The model was trained on high pressure capillary-rheometer data of an elastomer (70–120 °C; 10-5000 *1/s*), corrected for entrance losses and non-Newtonian profiles, and extended with synthetic points from a Carreau-Arrhenius fit to include the low-shear plateau. On test data, MVI achieved $R^2 = 0.99$ while preserving finite zero-shear viscosity. Independent validation on different materials across wider ranges gave $R^2 = 0.957–0.990$ without retraining, confirming strong generalization. To demonstrate its practical applicability, capillary-flow CFD simulations were carried out using both the MVI and Carreau-Arrhenius models. While each gave accurate predictions of the pressure-flow response, the MVI model required less computational effort because it avoids repeated exponential calculations. These findings highlight the MVI model as a novel, efficient, and practical solution for viscosity modeling in polymer processing and other fluid flow applications.

Keywords Viscosity · Symbolic Regression · Machine Learning · Shear-Thinning Fluids · Non-Newtonian Fluids

Introduction

The rheological behavior of fluids, particularly their viscosity under varying conditions, forms the basis for numerous industrial applications. Newtonian fluids exhibit a constant viscosity regardless of the applied shear rate, meaning their flow behavior is predictable and linear, as observed in fluids like water or air (Dolz et al. 2005). However, many fluids deviate from this behavior, displaying complex viscosity changes that depend on factors such as shear rate, temperature, and pressure. These are classified as non-Newtonian fluids (Chhabra and Richardson 2008). Among these, shear-thinning (pseudoplastic) fluids hold particular significance. These fluids demonstrate a decrease in viscosity with an increase in the applied shear rate. This phenomenon is attributed to the alignment or disentanglement of molecular structures, such as polymer chains, under shear stress (Hassan et al. 2022). A prime example of this behavior is seen in

✉ Mohammad Pourhosseinian
mohammad.pourhosseinian@tuwien.ac.at

✉ Bahram Haddadi
bahram.haddadi@chasecenter.at

1 Department of Mechanical and Aerospace Engineering, Politecnico di Torino, Torino, Italy

2 Institute of Chemical, Environmental & Biological Engineering, TU Wien, Vienna, Austria

3 Competence Center CHASE GmbH, Linz, Austria

4 Semperit Technische Produkte GesmbH, Research and Development Department, Wimpassing, Austria

5 Department of Energy, Politecnico di Torino, Torino, Italy

Published online: 07 March 2026

polymer melts, where viscosity decreases significantly during processing, enabling their efficient use in applications such as extrusion and molding (Salehi et al. 2018).

Several constitutive models have been proposed to describe shear-thinning behavior. The Carreau model is widely used because it accounts for both low- and high-shear Newtonian limits, capturing the transition between them (Wrobel 2020; Azeez and Bertola 2021). It has also been applied to study flow stability, for example in plane Couette flow (Tanmay et al. 2018). The Cross model is a simplified alternative, often applied in fields such as hemodynamics, where it can predict the distribution of wall shear stress and velocity fields in blood flow through the human aorta (Karimi et al. 2014) and polymer processing (Bair 2018), but it lacks the flexibility of Carreau in some cases. The Power Law model is mathematically straightforward and frequently used for polymer processing predictions (Marschik et al. 2017). However, it cannot describe Newtonian plateaus and predicts infinite viscosity at zero shear rate, which is problematic for applications like CFD simulations (Ruschak and Weinstein 2014) (Gołdasz and Sapiński 2015). Therefore, the Carreau model is suggested to be used to deal with this limitation of the Power Law model (Fayed et al. 2016).

The dependency of viscosity on temperature also plays a crucial role in non-isothermal flows, introducing nonlinearity to the viscosity of the fluid. In polymer processing, this is usually modeled with Arrhenius, Williams-Landel-Ferry (WLF), or Vogel-Fulcher-Tammann (VFT) relations. When polymer or drug-polymer melts are processed well above Tg, the viscosity is commonly described by combining an Arrhenius law for temperature dependence with a shear-thinning model such as Carreau or Carreau–Yasuda. This combined approach is widely applied in hot-melt extrusion and injection molding (Radwan et al. 2024; Rabhi et al. 2024). Near T_g, free-volume effects dominate and the WLF equation is preferred. It's used to generate master curves for rubber compounding, stiffness control in automated composites manufacturing, and hot-melt adhesive characterization (Budelmann et al. 2020; Mallamace et al. 2024). For amorphous polymers operated close to T_g (e.g., PS, PMMA), VFT capture the steep thermal sensitivity of zero-shear viscosity and are often used alongside Carreau-type shear-thinning in film- and fiber-processing models (Recondo et al. 2006; Popova and Surovtsev 2014; Chapman et al. 2021).

While classical viscosity models cannot take into account the effects of both shear rate and temperature on their own, to have an accurate non-linear model, temperature dependent models should be combined with shear rate dependent models, making the overall equation complex and non-linear. Consequently, a simpler and accurate approach is required to deal with such complexity.

Several attempts have been made to use Artificial Intelligence and Machine Learning techniques to predict the viscosity of non-Newtonian fluids. For example, Daniel R. Cassar used Neural Network method to predict the temperature dependency of the viscosity by predicting the fit parameters of the MYEGA equation (Cassar 2021). Multilayer Perceptron Neural Networks and Decision Trees have also been implemented in other studies to predict the viscosity of non-Newtonian fluids, showing excellent accuracy (Li et al. 2023). Classical Regression Techniques (CRT) and Neural Regression Techniques (NRT) were also used in order to predict the viscosity, by A.M. Elsharkwy et al., showcasing the accuracy of NRT compared to CRT (Elsharkwy and Gharbi 2001). Artificial Neural Network has also been implemented to predict the viscosity of black oil below bubble point, resulting in better performance compared to previously introduced models (Ayoub et al. 2007). The prediction of viscosity using Fuzzy Logic and Neural Networks was also investigated by Hajizadeh Y et al., showing the superiority of AI predictions compared to classical models (Hajizadeh 2007). Another study by Saadat et al. was done focusing on the selection of the most suitable viscosity model for a given data set of shear rate. They implemented a Rheology Informed Neural Network framework in which the algorithm was able to find the best model among 9 constitutive models introduced to it, that fit the shear rate data the best (Saadat et al. 2022).

Although all previous studies suggest high accuracy of Machine Learning algorithms, a key aspect that should be taken into account is the complexity of these algorithms in practice. The models are black boxes, require retraining for each dataset and application, and are slow to evaluate, which makes it difficult to use in CFD, process design and optimization, and real-time control. Most papers also fail to provide a single transferable formula, so results are not easily reproducible across materials and operating ranges. The aim of this study is to develop a simple yet accurate viscosity model using Artificial Intelligence that implicitly captures the effects of shear rate and temperature. This approach leverages the predictive accuracy of Machine Learning while ensuring that the resulting model remains efficient enough for practical use in Computational Fluid Dynamics simulations.

Experiments

To derive a nonlinear viscosity model as a function of both shear rate and temperature, and to obtain a suitable dataset for model training, rheometer measurements were carried

out (provided by Semperit) on a selected elastomer compound, which exhibits strong temperature and shear rate dependencies. In industrial applications, there are two main groups of rheometers that can be used to measure viscosity of elastomers. The first uses a device in which the fluid is sheared between two walls, one stationary, one moving, and the fluid is adhered to the moving wall and dragged along it (Kukla et al. 2017). The second forces the sample through a channel, either cylindrical or slit, such as a pressure-driven flow by a piston, as in high-pressure capillary rheometers (Mewis and Wagner 2011). High-pressure capillary rheometers are subdivided into Speed Control and Pressure Control types (Syrjälä and Aho 2012). In this study, viscosity data were collected using a Speed Control device, in which the piston imposes the flow rate and pressure curves are monitored. When a stable pressure curve is reached, a measurement point is taken, and the piston speed is increased to measure the next shear point. Experiments were performed using a high-pressure capillary rheometer, Rheograph 25/50 (Göttfert GmbH), in a temperature range starting from 70 °C to 120 °C and shear rate range from around 10 s^{-1} to 5000 s^{-1}, covering a valid range suggested in the applications of high-pressure capillary rheometers (Juster et al. 2014). Furthermore, the glass transition temperature of the used compound is around −50 °C. Since on round dies the pressure transducer is located at the entrance only, so the axial pressure drop along the capillary is not directly measured (Fig. 1)., therefore two dies were installed in parallel for entrance-loss correction. The primary round die had a length of 20 *mm* and a diameter of 2 *mm* (*L/D*=10:1). The secondary die had a length of 0.2 *mm* and served as a "zero-length" die for linear Bagley correction.

Measurement procedure was consistent across all conditions. At each temperature, piston speed was stepped from low to high to span the target shear-rate range. Data were recorded only after the pressure signal stabilized, and the barrel/die temperatures reached the set value. Standard capillary-rheometry assumptions were used during data extraction, namely fully developed and steady, isothermal, slip-free, incompressible, and laminar flow (Syrjälä and Aho 2012). The measured pressure was treated as the sum of fully developed and entrance contributions (Hopmann and Michaeli 2016):

$$p = p_l + p_e \tag{1}$$

where p_e is the entrance loss and p_l is the pressure drop along the capillary in *Pa*. Using the two-die Bagley method, p_e was obtained and subtracted to give p_l (Bagley 1957). The apparent wall shear stress follows from the corrected pressure drop and die geometry:

$$\tau_{app} = \frac{p_l R}{2L} \tag{2}$$

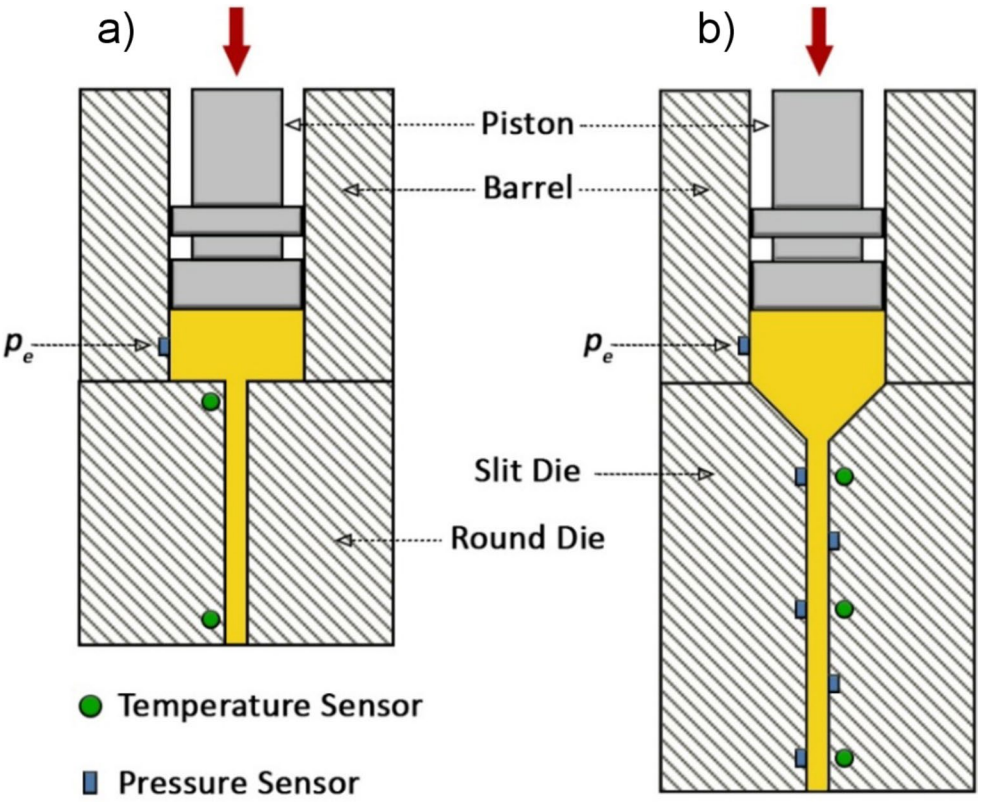

Fig. 1 (**a**) Round die and (**b**) Slit die configurations (Duretek et al. 2015)

where R is the radius of the capillary in *mm*, and L is the length of the capillary in *mm*. Equation 2 represents the apparent wall shear stress (τ_{app}). As discussed, the contribution of entrance effects should be considered and subtracted from the overall pressure loss along the capillary length. As a result of Bagley correction, true values of shear stress at the wall of the capillary can be obtained:

$$\tau = \frac{(p - p_e)R}{2L} \tag{3}$$

Various piston speeds are examined when taking measurements in a speed-controlled arrangement. Therefore, volumetric flow rate (Q) can be calculated at each measurement point by the following equation:

$$Q = \frac{\pi D^2}{4} V \tag{4}$$

where V is the piston speed in *mm/s* and D is the piston diameter in *mm*. Consequently, one can obtain the apparent values of the shear rates ($\dot{\gamma}_{app}$) at the wall as follows:

$$\dot{\gamma}_{app} = \frac{4Q}{\pi R^3} \tag{5}$$

The above formula can be used to calculate the shear rate for a Newtonian fluid (Laun 2004). But in a non-Newtonian fluid, the velocity profile is no longer parabolic and can be considered as a function of viscosity. To correct the apparent shear rate to account for non-parabolic velocity profile and non-Newtonian behavior, the Weissenberg-Rabinowitsch correction can be used (Rabinowitsch 1929):

$$\dot{\gamma} = \frac{3n + 1}{4n} \dot{\gamma}_{app} \tag{6}$$

where n is the derivative of $log\,(\tau)$ with respect to $log(\dot{\gamma}_{app})$. To obtain a stable local slope, $\tau(\dot{\gamma}_{app})$ was fitted in log-log space; although a second-order polynomial was generally adequate, a fourth-order polynomial is used and then differentiated to reduce gradient errors at certain shear-rate ranges (Syrjälä and Aho 2012).

By derivation of true values of wall shear stress and wall shear rate, correct viscosity measurement points can be reached, and true shear viscosity ($\eta\,(\dot{\gamma})$) can be calculated using:

$$\eta\,(\dot{\gamma}) = \frac{\tau}{\dot{\gamma}} \tag{7}$$

The main sources of uncertainties in this experiment were pressure measurement and the Bagley extrapolation, temperature control at the barrel and die, conversion of piston speed to flow rate, and the slope n in the Weissenberg-Rabinowitsch correction step. Selected tests were repeated to confirm repeatability.

Classical viscosity models

The rheological behavior of non-Newtonian fluids is governed by both shear-rate and temperature dependence. Capturing these effects in a single, reliable viscosity model is essential for polymer processing and flow simulations. One of the most widely used expressions is the Power Law model, which describes viscosity as a function of shear rate using only two fitting parameters. The equation can be written as:

$$\eta_{(\dot{\gamma})} = K\dot{\gamma}^{n-1} \tag{8}$$

The dimensionless exponent n is known as the flow behavior index, while K is the flow consistency index, with the unit of *Pa.s*. Its simplicity makes it attractive for analytical treatments and rapid fitting, but the model diverges at zero shear rate and fails to represent Newtonian plateaus at low and high shear rates. This limits its predictive capability in practical applications where a finite zero-shear viscosity is essential for numerical stability.

To overcome these limitations, more advanced models such as the Carreau (Carreau 1972) and Cross (Kim and Park 2018) equations were introduced. Both extend the Power Law by adding a transition term that accounts for the onset of shear thinning. The Carreau model introduces a time constant λ, which defines the critical shear rate at which non-Newtonian behavior emerges. It reads as:

$$\eta_{(\dot{\gamma})} = \eta_0(1 + (\lambda\dot{\gamma})^2)^{\frac{(n-1)}{2}} \tag{9}$$

where η_0 is the zero-shear viscosity, representing the value of Newtonian viscosity at the first plateau (i.e., when the shear rate is zero). By adding a viscosity limiter or extending the model (for example, using the Carreau-Yasuda equation (Yasuda 2005), it is possible to capture a high shear-rate plateau, representing the finite viscosity that some fluids exhibit at very high shear rates.

The Cross model, which is a simplified form of Carreau model, uses a characteristic shear stress τ to represent the same transition and can be written as:

$$\eta_{(\dot{\gamma})} = \frac{\eta_0}{1 + \left(\frac{\eta_0 \dot{\gamma}}{\tau^*}\right)^{1-n}} \tag{10}$$

Where η_0 is the Newtonian or zero shear viscosity, n is the power law index, and τ^* is the characteristic shear stress value. According to literature, τ^* mostly depends on the chemical properties of the fluid (Ferri et al. 2017) and determines the critical shear stress at which the transition to shear-thinning behavior occurs. Both models are capable of capturing Newtonian plateaus and shear-thinning regimes, but the Carreau formulation is particularly well-suited for polymer systems because it provides a smooth transition and has been shown to reproduce experimental data with high accuracy.

In addition to shear-rate effects, viscosity is strongly influenced by temperature. For most fluids, increasing temperature leads to a nonlinear decrease in viscosity. Several models have been developed to describe this behavior. The Arrhenius equation is one of the most widely applied, representing viscosity as an exponential function of the temperature. The equation can be expressed as:

$$\eta_{(T)} = \eta_a e^{\left(\frac{E_a}{R.T}\right)} \tag{11}$$

where η_a is the pre-exponential factor, which represents the viscosity at a reference temperature, E_a activation energy, and R the molar gas constant. Although its simplicity and effectiveness over moderate ranges, it tends to deviate near the glass transition temperature. Alternatives such as the WLF and VFT models improve accuracy close to the glass transition but add additional parameters and maintain an exponential form that increases computational cost.

In combined formulations, the zero-shear viscosity η_0 is typically expressed as a temperature-dependent function, while other parameters are treated as constant. Experiments show that η_0 often follows Arrhenius-type behavior (Tanguy et al. 1988) and, in some cases, can also be described by the WLF equation (Rudolph et al. 2016). Consequently, the shear rate and temperature dependency models can be combined by replacing the η_0 term by the temperature models. Table 1 presents the final combination of the discussed models. This approach is widely adopted in polymer rheology, as several studies have shown that the other parameters are only weakly dependent on temperature over typical processing ranges, whereas η_0 exhibits strong temperature sensitivity and dominates the thermal response of viscosity (Tanguy et al. 1988; Vlachopoulos and Polychronopoulos 2011).

This coupling improves accuracy but results in bulky multi-variable expressions, with repeated exponential evaluations that increase computational cost in CFD.

For the present work, the Power Law model was unsuitable because it cannot represent Newtonian plateaus, while the Cross model gave poorer agreement with the experimental data. The WLF model was also excluded, since the glass transition of the studied compound lies far below the investigated temperature range. In contrast, the Carreau-Arrhenius model is well established for polymeric systems, as it combines shear-rate dependence with a physically consistent temperature effect. For these reasons, it was selected as the baseline for further analysis and comparisons.

The fitting parameters of the viscosity models were obtained through nonlinear least-squares optimization of the experimental dataset. The equation is expressed as:

$$RSS = \sum_{i=1}^{n} \left(\left[f\left(x_i; b\right) - y_i \right]^2 \right) \rightarrow \min_b RSS\left(b\right) \tag{12}$$

where f represents the model function, and specifically the viscosity models. Shear rate and temperature are independent variables, while b represents model variables such as time constant or zero shear viscosity. The data points are illustrated by x_i and y_i. This method minimizes the residual sum of squares (RSS) between measured and predicted viscosities, ensuring the best fit of model parameters (Aşıkgil 2017). To maintain physical consistency, parameter bounds and constraints were applied using the lmfit library in Python, which also provided fit statistics (e.g., reduced chi-squared, AIC, R^2) for accuracy assessment (Newville et al. 2014).

Table 1 Overall representation of classical viscosity models as a function of shear rate and temperature

	Arrhenius	WLF
Carreau	$\eta_0 e^{\frac{E}{RT}} \left(1 + (\lambda\dot{\gamma})^2\right)^{\frac{n-1}{2}}$	$\eta_0 e^{\left(-\frac{c_1(T-T_g)}{c_2+(T-T_g)}\right)}(1+$
Cross	$\frac{\eta_0 e^{\frac{E}{RT}}}{1+\left(\frac{\eta_0 e^{\frac{E}{RT}}\dot{\gamma}}{\tau^*}\right)^{1-n}}$	$\frac{\eta_0 e^{\left(-\frac{c_1(T-T_g)}{c_2+(T-T_g)}\right)}}{1+\left(\frac{\eta_0 e^{\left(-\frac{c_1(T-T_g)}{c_2+(T-T_g)}\right)}\dot{\gamma}}{\tau^*}\right.}$
Power Law	$\eta_0 e^{\frac{E}{RT}} \dot{\gamma}^{n-1}$	$\eta_0 e^{\left(-\frac{c_1(T-T_g)}{c_2+(T-T_g)}\right)} \dot{\gamma}^{n-1}$

Symbolic regression

Symbolic Regression is a machine learning method that falls under the category of evolutionary algorithms. It is a unique approach where a mathematical expression is derived to best represent the given data. Unlike traditional regression or data-driven methods, which rely on predefined objective functions, symbolic regression can generate analytical formulas directly from the data without requiring prior knowledge of the mathematical representation of the model function. This capability significantly improves the interpretability, generalizability, and flexibility of the model-building process, making it a powerful tool for discovering meaningful relationships in complex datasets (Hou et al. 2024). In this work, symbolic regression was used as it nicely aligns with the goals and purpose of the study. It was used within a suitable computational setup to create a unique viscosity equation that requires low computational effort and is therefore easy to use in Computational Fluid Dynamics (CFD) simulations.

Symbolic Regression follows a hierarchical approach in which binary, unary, and other mathematical operators are predefined, forming a tree-structured foundation in which candidate equations are constantly evaluated and their fitness to the input data will be observed (Liu et al. 2024). Due to the evolving nature of the Symbolic Regression algorithm, it is typically implemented using evolutionary algorithms, particularly Genetic Programming (GP) (McConaghy 2011). GP provides a method for representing data behavior through mathematical formulas by exploring a vast range of possible equations. This process occurs through an evolutionary approach, where different mathematical structures are iteratively tested and refined to find the best fit for the data (Angelis et al. 2023). Based on GP principles, symbolic mathematical equations are constructed using a predefined set of operators, and the equations that do not represent input data behavior accurately are eliminated. Figure 2 illustrates the tree-structured representation of a Symbolic Regression algorithm (Angelis et al. 2023).

The structure consists of primitive functions and terminals. Primitive functions include logical operators, mathematical functions, or customized user-defined functions, while terminals represent the inputs and numerical constants. The overall expression in Fig. 2 can be represented as a rooted tree, where the internal points of the tree are primitive functions, and external points are terminals. A more detailed explanation of Genetic Programming principles can be found in the work of Koza J. (Koza 1994).

There are various frameworks available that can be used in order to implement Symbolic Regression such as GPTIPS MATLAB toolbox (Dominic et al. 2010), AI Feynman that combines Symbolic Regression with Neural Networks (Udrescu and Tegmark 2020), Eureqa software which its underlying principles are elaborated by Schmidt, M., & Lipson, H. (Schmidt and Lipson 2009), and PySR, an open-source symbolic regression library using a multi-population evolutionary algorithm and Julia's SymbolicRegression.jl backend (Cranmer 2023). In the present work, PySR was chosen due to its support for parallelization, configurability, flexibility, seamless integration within the Python ecosystem, and its performance and efficiency.

In the evolutionary algorithm of PySR, multiple populations are first defined, and the inner loop of algorithm acts on each population independently. The principle is based on tournament selection for individual selection (Brindle 1980; Goldberg and Deb 1991), and to generate new individuals,

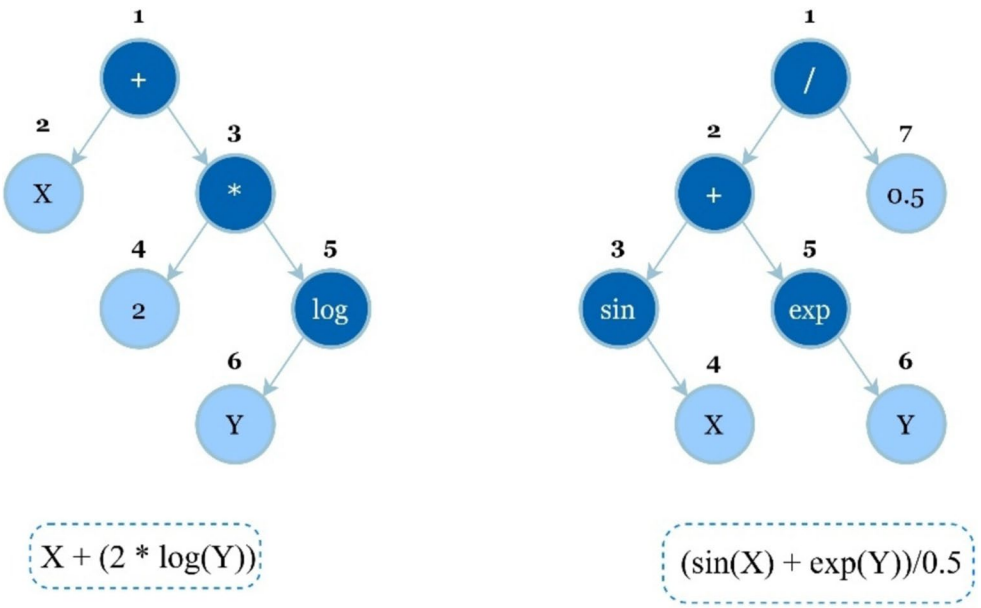

Fig. 2 Tree-Shaped symbolic regression algorithm structure

mutations and crossovers are performed as can be observed in Fig. 3. The detailed explanation of PySR algorithm can be found in the original paper published by Miles Cranmer (Cranmer 2023).

The loss function utilized in the present work is Mean Squared Error (MSE) defined as:

$$MSE = \frac{1}{n}\sum_{i=1}^{n}(\gamma_i - \widehat{\gamma}_i)^2 \tag{13}$$

In the abovementioned equation, n is the total number of data points, i corresponds to the index of each individual data point, $\widehat{\gamma}$ is the predicted value of the i-th data point and γ is the correct answer.

Data analysis

The first and crucial step in every Machine Learning algorithm is to prepare the input data appropriately to prevent overfitting, underfitting, divergence problems, etc., by excluding outliers, artifacts, etc. Due to the data-driven nature of these algorithms, particularly Symbolic Regression, the input data should be prepared in a way that enables the model to capture all necessary viscosity regions such as Newtonian plateaus, transition regions and pseudoplastic regions. Due to the fact that the compound used in this work exhibits constant viscosity at a very low shear rate, which is almost outside of the range in which the High-Pressure Capillary Rheometer device is able to measure the viscosity correctly, all experimentally obtained measurement points lie within the pseudoplastic or shear-thinning region. Therefore, by using this dataset to train the model, the final equation can only account for shear-thinning behavior and no Newtonian plateau or transition region will be covered. Furthermore, a portion of the available data set should also be used as a test set, to ensure the final discovered equation is able to perform correctly on the unseen data points. Therefore, the final measurement points were divided into two different datasets: training and test. To deal with the abovementioned challenges, special attention should be given to the training set.

To overcome the limitations of our measurement device and ensure the training set includes all relevant viscosity regions, 70% of the measured dataset was used as a basis for generating synthetic data points. This approach is consistent with common practices found in the cross-validation literature, where empirical studies suggest that reserving 20–30% of the data for testing often yields optimal generalization performance (Gholamy et al. 2018). The Carreau-Arrhenius model was fitted to this data set by methods explained in Sect. 3, and after extracting the fit parameters, a data set of approximately 2000 points were generated. The data set covers the first Newtonian plateau, transition and shear-thinning region. Additionally, the viscosity value predicted by the Carreau-Arrhenius model at exactly zero shear rate was included in the data set to make sure that the algorithm finds an equation in which the viscosity value does not approach infinity at zero shear rates. In this case, the Carreau-Arrhenius model served not only as the foundational basis for the final equation but also as a structural constraint that implicitly helps manage physical consistency and robustness in the presence of potential noise or variation in the data. The remaining 30% of the original measurement points were used as test set to ensure the generality of the final equation and capability to be fit to the unseen data.

An interesting extension of the present framework would be to apply symbolic regression directly to pressure-flow (or apparent-shear-rate) formulations, enabling model identification without explicit WR post-processing and potentially improving the interpretability of fitted parameters. This

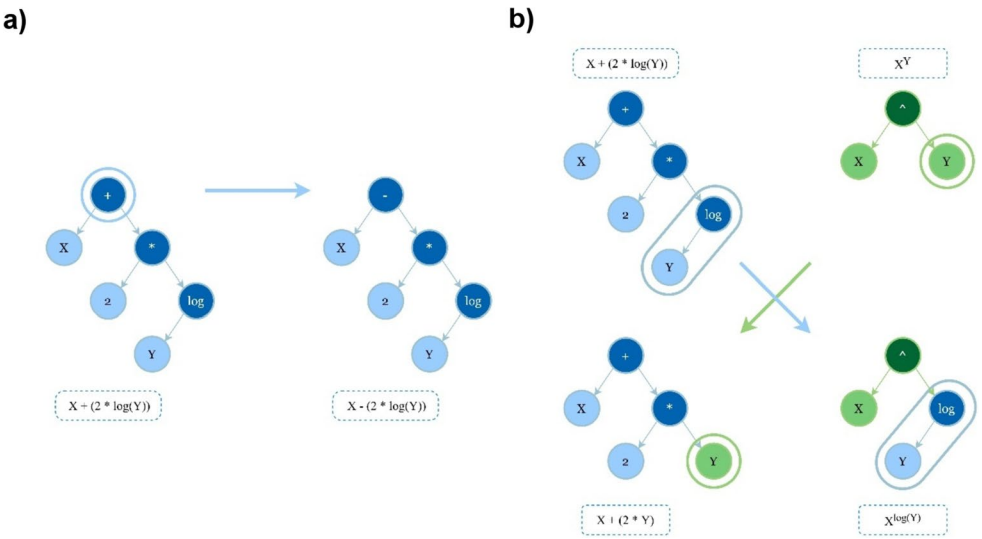

Fig. 3 (**a**) Mutation applied to the expression tree. (**b**) Crossover applied to two different expression trees

would require a different identification strategy and validation workflow and is therefore left for future work.

Independent dataset acquisition

To further evaluate the generalizability and robustness of the final viscosity model, an independent dataset was introduced. This dataset consists of viscosity measurements for three distinct thermoplastic polymers: polypropylene (PP), polystyrene (PS), and acrylonitrile butadiene styrene (ABS). These materials exhibit different rheological characteristics compared to the elastomer compound used for model training. Moreover, the measurements were carried out under more extreme conditions, covering broader ranges of shear rates and temperatures than those used in the original experiments. This design allows the evaluation of the model's extrapolation capability and ensures its applicability to a wider class of shear-thinning fluids. Figure 4 shows viscosity curves for PP, PS, and ABS across a wide range of shear rates and temperatures. All three polymers display clear shear-thinning behavior, with viscosity decreasing as shear rate increases. The temperature effect is also evident, as the viscosity shifts downward with increasing temperature. These datasets span shear rates from 0.06 to 630 *1/s* and temperatures between 180 and 260 °C, which represent much more extreme conditions than those used in the base experiments.

The shear viscosity of these materials was measured by using an Anton-Paar MCR 302 plate-plate rheometer equipped with an electrically heated thermostating unit. Measurements were performed in a parallel-plate mode under nitrogen. For sample preparation, the polymeric materials were compression-molded into disc-shaped specimens with a diameter of 25 *mm* and a thickness of 1 *mm*. The samples were placed between two parallel circular plates with a diameter of 25 *mm*, with the lower plate remaining stationary while the upper plate rotated at controlled angular velocities. For each material, measurements were performed at three temperatures. Frequency-sweep tests were performed within the linear viscoelastic region, with the angular frequency varied between 0.1 and 121 *rad/s*. The Cox-Merz rule was employed to convert oscillatory data to steady-shear viscosity data.

CFD simulation

To verify the effectiveness of the proposed Multi-Variable Implicit (MVI) viscosity model in practical flow simulations, CFD studies were carried out using OpenFOAM® v2006. The objective was to test the model's ability to reproduce shear-rate and temperature-dependent viscosity effects, including viscous heating, and to compare its performance with classical models under conditions identical to the experimental setup.

For this purpose, the incompressible pimpleFoam solver was extended with a scalar transport equation for temperature to resolve non-isothermal effects and with viscous dissipation to account for heat generation due to shear. Within this solver, the proposed MVI model and the Carreau-Arrhenius model were implemented to allow direct comparison under identical conditions. To ensure numerical robustness, bounded schemes were used to prevent solver instability.

The computational domain was based on the high-pressure capillary viscometer used in the experiments (Sect. 2). The geometry consisted of a piston section with 15 *mm* diameter connected to a capillary die of 20 *mm* length and 2 *mm* diameter, giving an L/D ratio of 10. A fixed inlet velocity of 1.78 *mm/s* was set to represent piston motion, while the outlet was maintained at atmospheric pressure. No-slip boundary conditions were applied at all walls. The inlet and the wall surfaces maintained at a constant temperature of 80 °C, consistent with experimental conditions (Fig. 5a).

Meshing was performed using the blockMesh utility in OpenFOAM®. Following a mesh independence study, a structured hexahedral grid of 44,400 cells was adopted, providing accurate resolution of near-wall velocity gradients and pressure drop along the die, while keeping computational cost manageable (Fig. 5b). All simulations were performed on an Intel® Core™ i7-10700 CPU using a single core.

Results and discussion

In this section, the corrected viscosity measurements of the elastomer compound are presented, and the final derived equation is introduced. The new model is not intended to introduce new rheological physics but to provide a numerically efficient surrogate for the well-established shear-rate and temperature-dependent behavior classically captured by Carreau-Arrhenius and Cross-WLF-type models. Its contribution lies in offering a single closed-form expression that simultaneously accounts for shear rate and temperature, with reduced mathematical complexity and improved fitting efficiency. The derived equation is compared with classical viscosity models in terms of mathematical structure and computational cost, and its performance is assessed by fitting to the elastomer data as well as to independent datasets for three thermoplastic materials. Finally, the model is implemented in Computational Fluid Dynamics (CFD) simulations to evaluate its predictive capability in a realistic flow configuration.

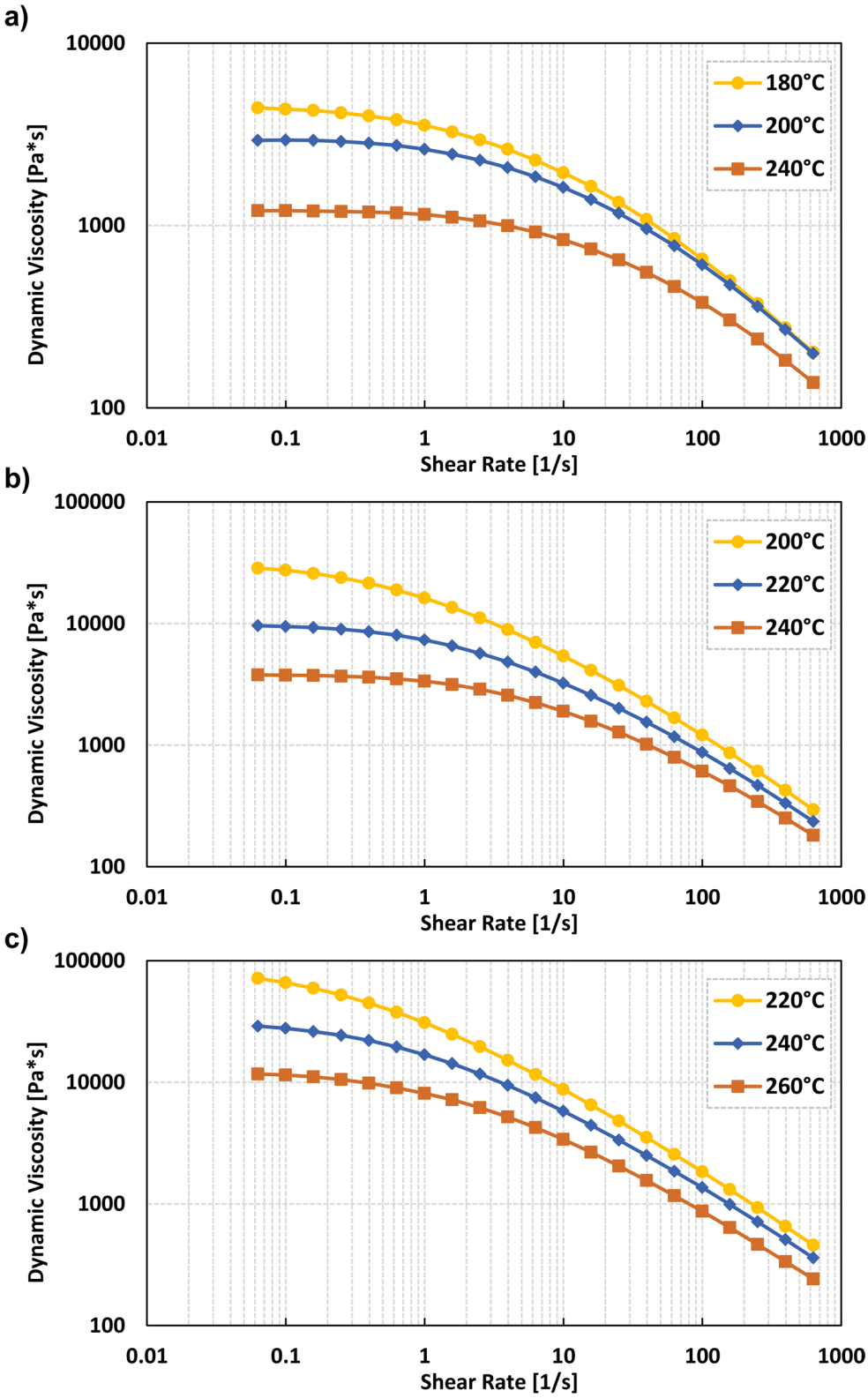

Fig. 4 Viscosity measurements of independent validation datasets under varying shear rates and temperatures: (**a**) Polypropylene (PP) (**b**) Polystyrene (PS) (**c**) Acrylonitrile Butadiene Styrene (ABS). The plot is in logarithmic scale

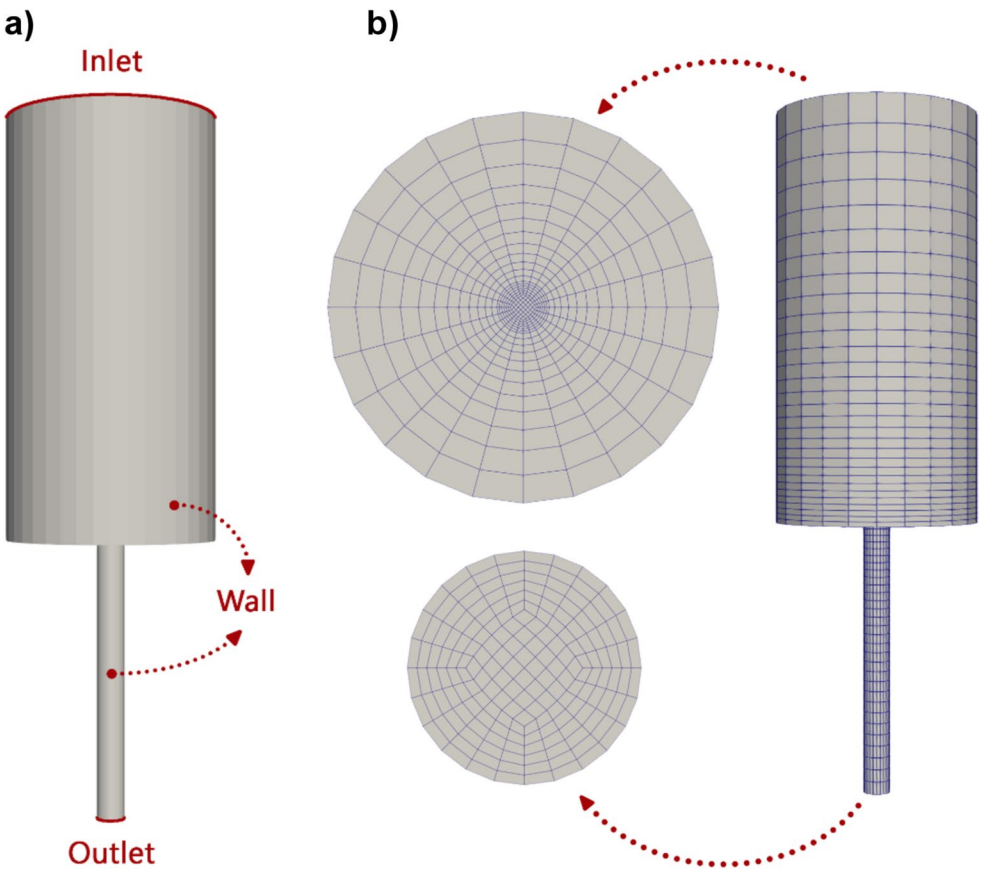

Fig. 5 (**a**) Geometry with boundary setup and (**b**) generated mesh with side, top and bottom view

Viscosity measurements

The experimental data was corrected for entrance pressure losses and the non-Newtonian fluid velocity profile. As mentioned earlier, the device used in the experiments features a round die, which does not allow pressure transducers to be installed along the fluid flow. Therefore, the pressure was measured at the inlet, and the Bagley correction was applied to account for entrance effects. Additionally, while the initial equations for fluid flow inside the capillary were based on the assumption of a Newtonian fluid, the Weissenberg-Rabinowitsch correction was applied to adjust for the non-Newtonian behavior of the compound.

Bagley correction

Since the experimental setup has two round capillary dies arranged in parallel, a linear Bagley correction is applied to the measurement points to correct for entrance pressure drop. Due to the high number of measurement points, only a selection is shown in figure 6. After obtaining the value of p_e, the apparent shear stress can be corrected. In Figure 6a the measured pressure drops at different apparent shear rates are plotted for two capillary dies with different L/D ratios. The lines are extrapolated to an effective L/D of zero to obtain the entrance pressure loss, which is then subtracted from the measured pressure to isolate the true pressure drop along the capillary. As shown in Figure 6, applying the Bagley correction reduces the apparent shear stress and viscosity because it removes entrance losses. This adjustment shifts the curves downward, giving more realistic shear stress and viscosity values.

Weissenberg-Rabinowitsch correction

The final step to achieve true viscosity values out of measurement data is to account for non-parabolic velocity profile which arises due to non-Newtonian behavior of the compound. Weissenberg-Rabinowitsch (WR) Correction is applied to correct apparent shear rate values. Figure 7 illustrates the effect of the WR correction on the viscosity data. The curves before and after the correction are shown for comparison. As noted earlier, the Bagley correction shifts the data downward by removing the entrance pressure contribution, thereby reducing the apparent shear stress and viscosity. Afterward, applying the WR correction adjusts the shear rate to account for the non-parabolic velocity profile of a non-Newtonian fluid. This correction shifts the data to the right, since the true shear rates are higher than the apparent values. As a result, both shear stress and viscosity

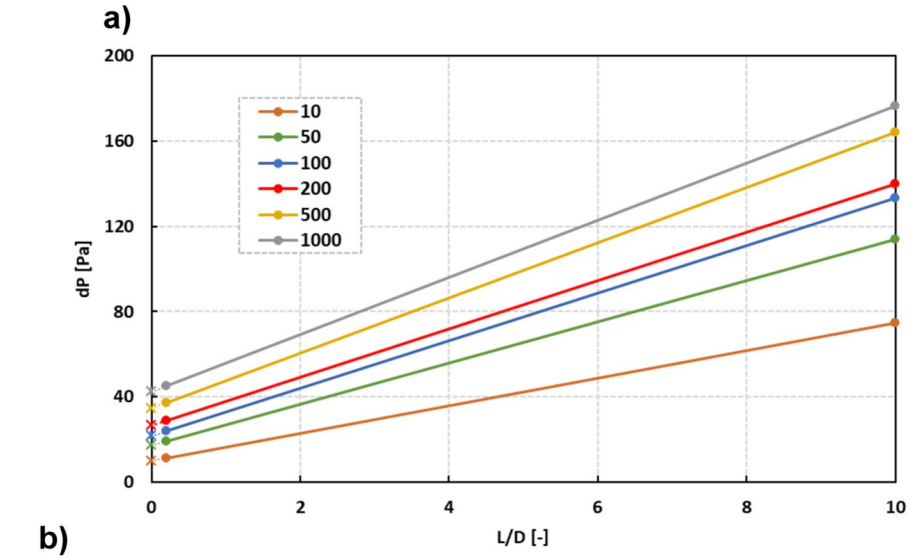

Fig. 6 (**a**) Bagley plot and linear extrapolation to obtain entrance pressure drop at 100 °C for different shear rates in range of 10–1000 *1/s*. (**b**) True shear stress and viscosity versus apparent shear rate and viscosity curves. The plot is in logarithmic scale

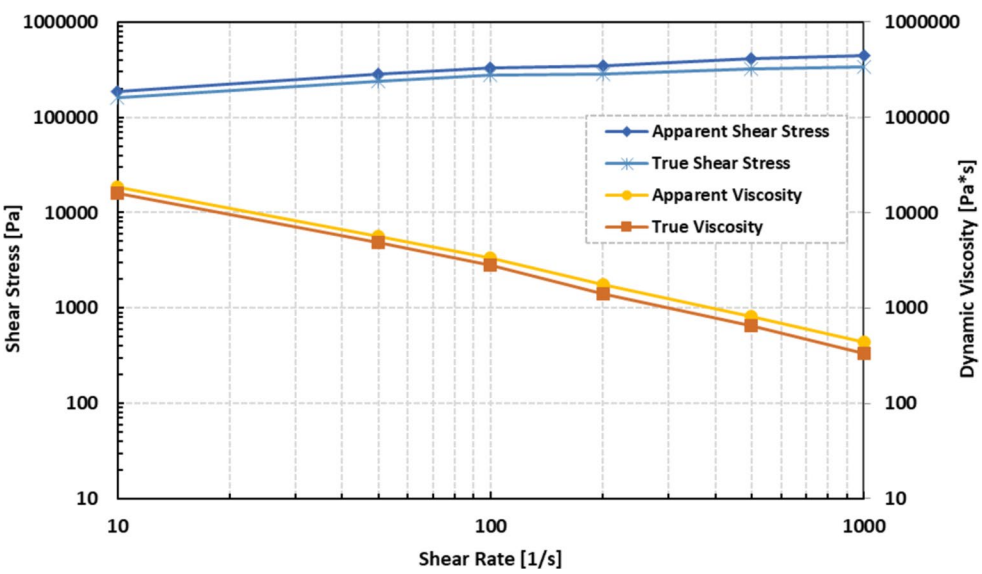

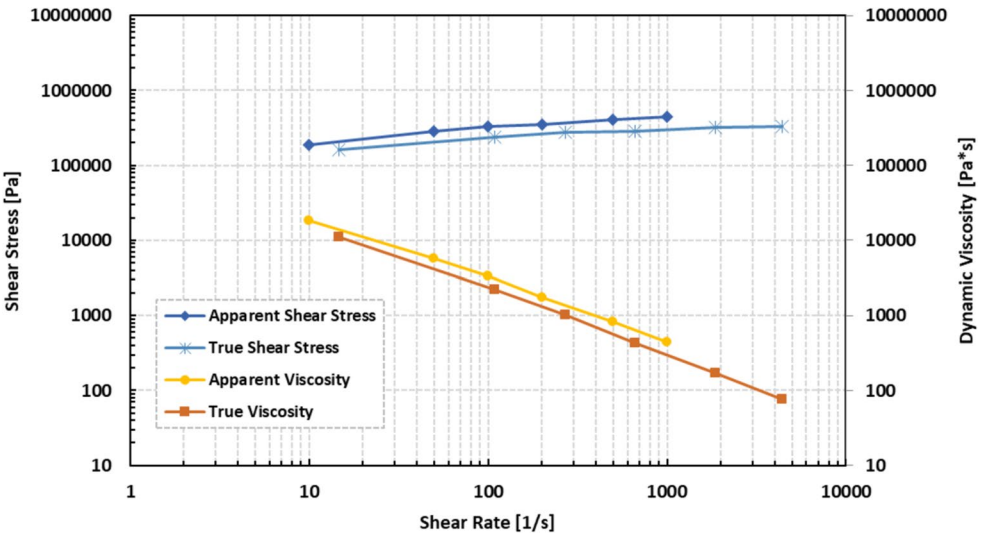

Fig. 7 Weissenberg-Rabinowitsch corrected measurement points. It should be noted that Bagley correction is also visible in this plot. The plot is in logarithmic scale

are repositioned along the shear-rate axis, yielding the final corrected values. This step is essential to obtain physically consistent viscosity values for shear-thinning fluids. Figure 8 illustrates the final true viscosity values obtained after applying both Bagley and WR corrections at different temperatures. The corrected curves show the expected shear-thinning behavior, where viscosity decreases as shear rate increases. In addition, temperature dependence is observed where viscosity decreases with increasing temperature across the entire shear-rate range. Together, these trends confirm that the corrections yield consistent and physically meaningful viscosity data, forming the basis for subsequent model fitting.

The new viscosity model

In this work, symbolic regression is used as an offline model-design tool to derive a Multi-Variable Implicit (MVI) viscosity model with all features needed for implementation in CFD frameworks. Rather than aiming to discover new rheological mechanisms or serving as a continuously retrained predictive model, symbolic regression (using PySR library) is employed to search a constrained space of dimensionally consistent algebraic expressions and identify a implicit constitutive equation that reproduces the known shear-rate and temperature dependence of polymer melts with minimal algebraic complexity. Once this functional form has been selected, it is fixed and subsequently used like any other empirical viscosity law: for each fluid, only a small set of coefficients is re-fitted by standard curve-fitting, and no additional machine-learning or symbolic-regression step is required. To ensure physically meaningful and computationally efficient expressions, the symbolic regression process was constrained using a specific configuration. PySR was limited to a restricted set of binary operators (*, -, +,/, ^), with exponentiation constrained to the range (9, 3) to control power values. To avoid overly complex forms, nested exponentials were disallowed. The search space was managed using a population size of 500 distributed across 24 populations. A dimensional-penalty term was used to favor expressions that respect the expected units of viscosity and shear-rate with a constraint penalty of 10^3. The final equation has been tested on the unseen data set (test set) and showed excellent accuracy and is represented in Eq. 14.

$$\eta\left(\dot{\gamma},T\right)=\frac{\left(c_1-T\right)c_2}{c_3+\left(\dot{\gamma}^2(\dot{\gamma}+c_4)^{c_5}\right)} \tag{14}$$

The MVI viscosity model has 5 fit parameters that are named C_1 to C_5 which need to be obtained with curve fitting algorithms, in the same way that parameters such as n, λ, and η_0 are identified for classical Carreau- or Cross-type models, making the model general to be applied on any shear-thinning fluid. These coefficients are phenomenological rather than directly measurable microscopic quantities, and their role is to shape the viscosity surface in a controlled and dimensionally consistent way. In the present formulation, C_1 $[K]$ can be referred to as a reference temperature for normalization purposes; C_2 $[Pa/(K.s^{(1+C5)}]$ may be seen as a thermo-rheological coefficient, reflecting the combined influence of temperature and time on viscosity; C_3 $[1/s^{(2+C5)}]$ can represent a structural relaxation rate, associated with the fluid's internal response time to deformation; C_4 $[1/s]$ functions as a basic shear rate constant affecting the shear-thinning behavior; and C_5 (dimensionless) acts as a time-scaling exponent, and is the most sensitive parameter, significantly shaping the model's responsiveness to input variations. The model has a simplified mathematical representation and exponential terms available in classical models were eliminated, increasing the efficiency of the proposed model.

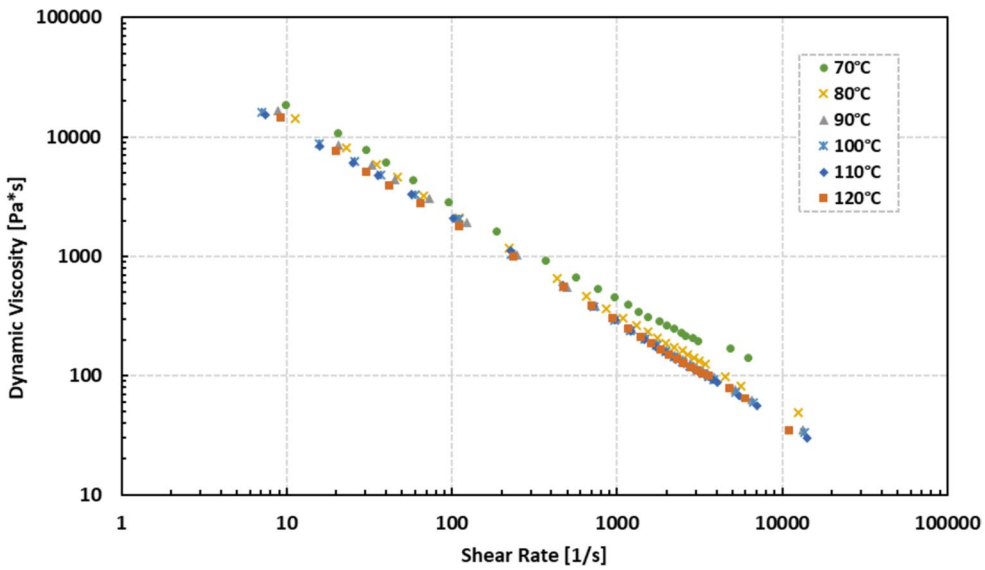

Fig. 8 Final measurement points overview. The plot is in logarithmic scale

Exponential operations are notably more computationally expensive than basic arithmetic operations such as addition, multiplication, and division. While basic arithmetic typically incurs very low latency on modern CPUs (around 3–13 cycles), transcendental functions like exp() and log() often require 50–200 + cycles due to their complexity. By replacing these costly operations with simpler algebraic expressions, the MVI model inherently reduces computational demand, resulting in improved efficiency during evaluation (Fog and others 2011). Furthermore, the model accounts for the effects of both shear rate and temperature implicitly and there will be no need to combine it with any other viscosity model. The fitted coefficients reported for the elastomer are calibrated for the experimental temperature window (70–120 °C). Within this range, the temperature factor in the model remains positive and the predicted viscosity is strictly positive. Moreover, Within the augmented training domain (plateau, transition, and shear-thinning regions generated as described in Sect. 5), the proposed MVI equation reproduces all relevant viscosity regimes, including a finite zero-shear viscosity. A mathematical comparison of the proposed MVI viscosity model with classical viscosity models is illustrated in Table 2.

Fit results

As explained in previous sections, the Carreau-Arrhenius model was selected as the classical reference because it is widely used for polymer melts and was also used to generate the synthetic dataset of 2000 points employed during the symbolic-regression stage. The MVI model was not constrained to reproduce the Carreau-Arrhenius functional form; instead, it was selected only on the basis of accuracy and algebraic simplicity. When fitted to the elastomer data, the final MVI expression gains accuracy comparable to that of the Carreau-Arrhenius model, while avoiding exponential temperature factors and combining the effects of shear rate and temperature within a single implicit law. In Fig. 9, the models are shown within the fitted range, where both closely follow the experimental points. They successfully capture the shear-thinning behavior of the compound as well as its dependence on temperature. Figure 10 shows extrapolation beyond the tested shear-rate range. Here, both models remain stable at low shear rates and capture the expected Newtonian plateau.

Both models demonstrate excellent accuracy when evaluated on the test set. The MVI model, in particular, achieves an R^2 score of 0.99, a Bayesian Information Criterion (BIC) of 1187, and a Root Mean Squared Standardized Residual (RMSSR) of 1.00118. Figures 11 and 12 present the results in two-dimensional contour form, providing a clearer view of how viscosity varies simultaneously with shear rate and temperature. Temperature effects are most pronounced at low shear rates, where viscosity changes strongly with temperature, and they become less significant at high shear rates. In Fig. 12, the extrapolated results are shown, where the Newtonian plateau is visible and the influence of temperature in this region can also be observed. The MVI model reproduces the overall temperature shift factors correctly, while yielding a slightly different but still physical temperature dependence in the Newtonian region. Derived fit parameters of both models for the tested polymer viscosity data are represented in Tables 3 and 4.

To assess the extrapolation capability and generalization performance of the proposed model, it was tested on an independent dataset consisting of three thermoplastic materials: polypropylene (PP), polystyrene (PS), and acrylonitrile butadiene styrene (ABS). These materials differ significantly in rheological behavior compared to the elastomer used during model development and were measured under a wider and more extreme range of temperatures and shear rates. This validation step was designed to evaluate the performance of the model beyond the domain it was originally trained on.

The fit results obtained using the MVI viscosity model for each of the three materials are presented in Fig. 13. The model was applied directly, without any retraining, and was able to accurately capture the shear-thinning behavior and temperature sensitivity across all three cases. It can be seen that the MVI model reproduces the shear-thinning regime, the transition range, the Newtonian plateau, and the temperature dependence for these polymers. This demonstrates

Table 2 Comparison of mathematical expressions of all models including the ML-based implicit multivariate viscosity model

	Arrhenius	WLF
Carreau	$\eta_0 e^{\frac{E}{RT}}\left(1+(\lambda\dot{\gamma})^2\right)^{\frac{n-1}{2}}$	$\eta_0 e^{\left(-\frac{c_1(T-T_g)}{c_2+(T-T_g)}\right)}(1+$
Cross	$\frac{\eta_0 e^{\frac{E}{RT}}}{1+\left(\frac{\eta_0 e^{\frac{E}{RT}}\dot{\gamma}}{\tau^*}\right)^{1-n}}$	$\frac{\eta_0 e^{\left(-\frac{c_1(T-T_g)}{c_2+(T-T_g)}\right)}}{1+\left(\frac{\eta_0 e^{\left(-\frac{c_1(T-T_g)}{c_2+(T-T_g)}\right)}\dot{\gamma}}{\tau^*}\right.}$
Power Law	$\eta_0 e^{\frac{E}{RT}}\dot{\gamma}^{n-1}$	$\eta_0 e^{\left(-\frac{c_1(T-T_g)}{c_2+(T-T_g)}\right)}\dot{\gamma}^{n-1}$
MVI Viscosity Model	$\frac{(c_1-T)c_2}{c_3+(\dot{\gamma}^2(\dot{\gamma}+c_4)^{c_5})}$	

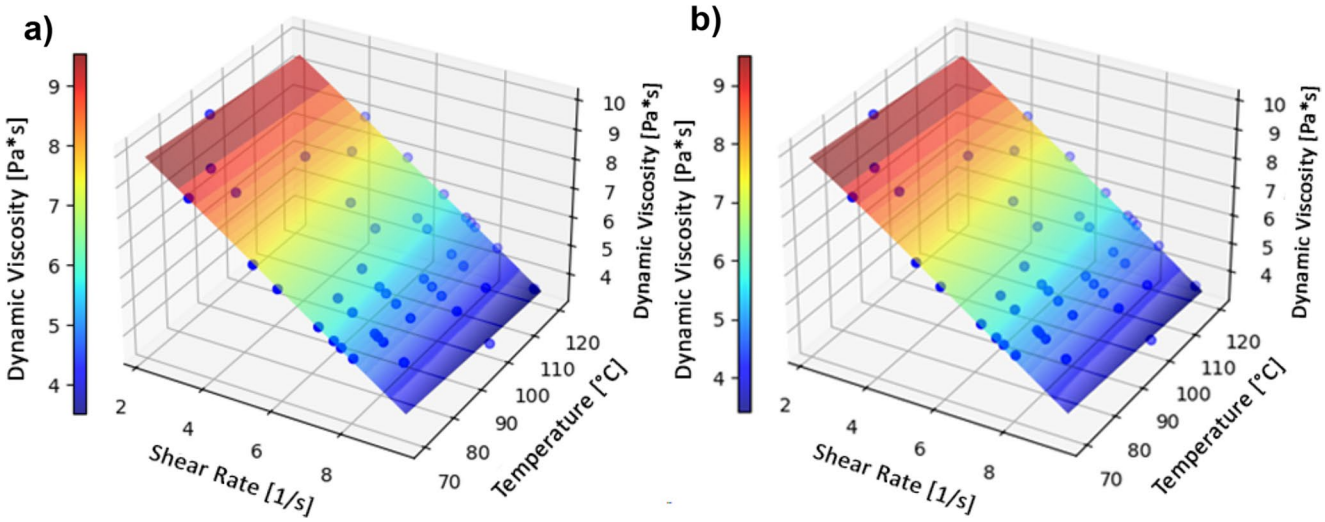

Fig. 9 (**a**) Carreau-Arrhenius model fit results on the test set. (**b**) MVI Viscosity model fit results on the test set

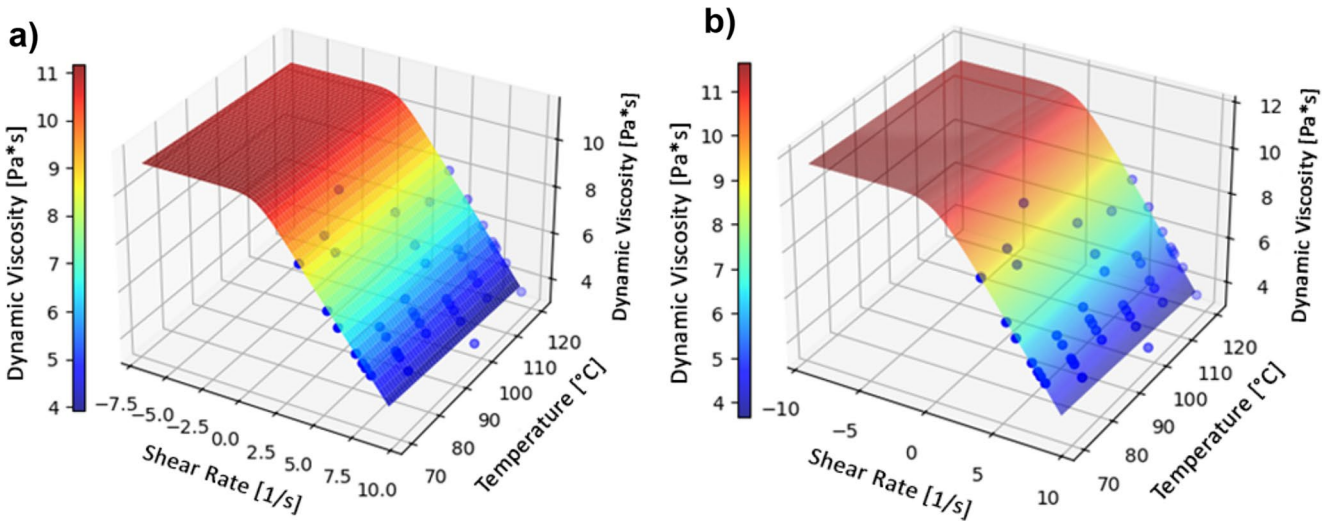

Fig. 10 (**a**) Carreau-Arrhenius model extrapolation fit result on the test set. (**b**) MVI Viscosity model extrapolation fit result on the test set

that the equation identified from the elastomer data is not utilized to a single fluid but can serve as a generic correlation form for a broader class of polymer melts and solutions.

A quantitative comparison between the MVI model and the independent test data is summarized in Table 5, which reports the Bayesian Information Criterion (BIC), R^2, and Root Mean Squared Standardized Residual (RMSSR) for each material. The MVI model achieves high R^2 values (0.957–0.990) and low RMSSR values close to unity across three different thermoplastic materials, indicating strong predictive accuracy and robust generalization performance.

In addition to accuracy, the efficiency of the fitting process was also evaluated. To validate this aspect, the derived model was tested on the three independent datasets and compared to the Carreau-Arrhenius model, with both fittings performed using the lmfit library in Python. As summarized in Table 6 the MVI model required up to five times fewer iterations to converge, while still achieving comparable accuracy. This shows that the simpler algebraic structure of the MVI model not only reduces the cost of viscosity evaluations in CFD but also makes the calibration stage more efficient, which is relevant in workflows where model parameters must be repeatedly updated.

CFD results

The extended pimpleFoam solver was used to simulate flow through the high-pressure capillary viscometer. Simulations were performed using both the proposed MVI viscosity model and the Carreau-Arrhenius model, enabling direct comparison under identical conditions. Table 7 illustrates the pressure drop comparison along the capillary die. Both

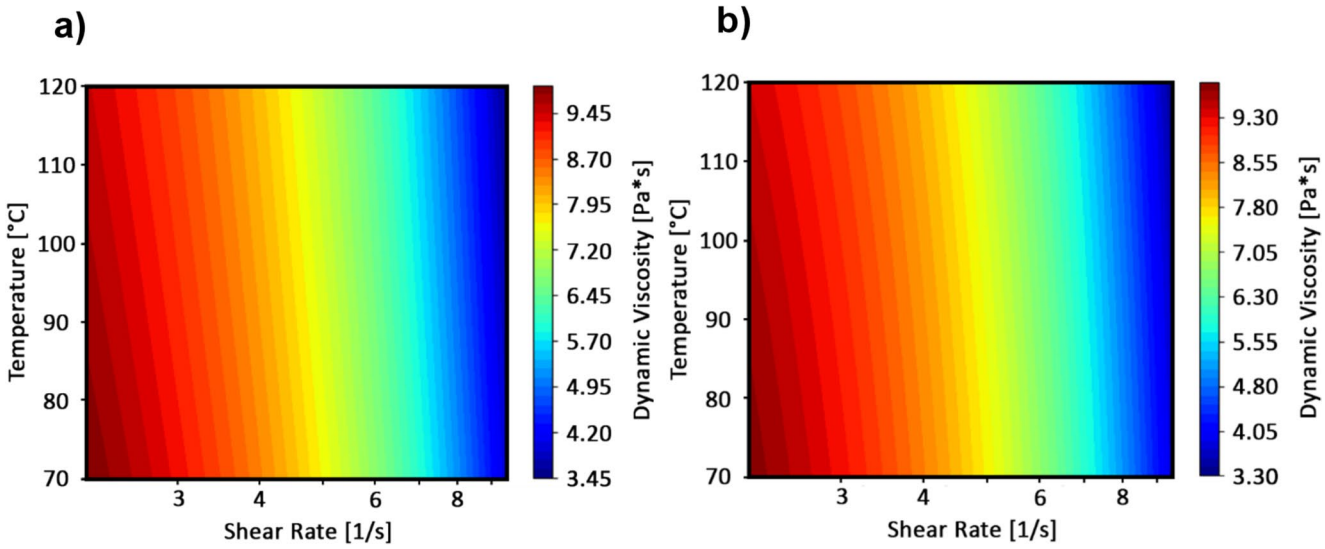

Fig. 11 (**a**) Carreau-Arrhenius viscosity contour on the test set. (**b**) MVI Viscosity model viscosity contour on the test set

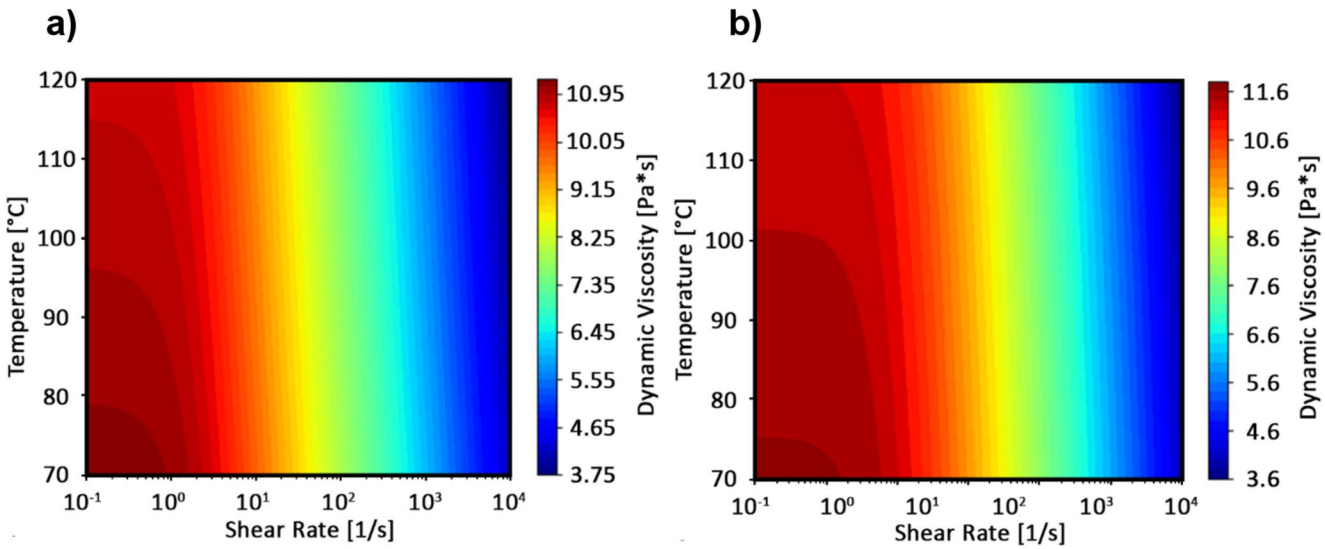

Fig. 12 (**a**) Carreau-Arrhenius model extrapolation of the viscosity contour on the test set. (**b**) MVI Viscosity model extrapolation of the viscosity contour on the test set

Table 3) Derived variables of Carreau-Arrhenius Viscosity Model

n [-]	Carreau-Arrhenius
	0.185
E [J/mol]	9484
η_0 [Pa. s]	2592
λ [s]	0.535

Table 4) Derived variables of MVI Viscosity Model

C_1 [K]	MVI Viscosity Model
	492.12
C_2 [Pa/(K.s$^{(1+C5)}$]	903.5
C_3 [1/s$^{(2+C5)}$]	1.19
C_4 [1/s]	0.525
C_5 [-]	−1.16

models reproduced the experimentally observed pressure drop with excellent agreement. The pressure drop predicted by the MVI model deviated by less than 0.6% from experimental values, while the Carreau-Arrhenius model deviated by around 9%. This confirms that the simpler algebraic MVI correlation can reproduce the macroscopic flow response at least as accurately as a classical temperature-dependent viscosity law. Velocity profiles across the die cross-section were also consistent between the two models, with both capturing the expected flattened velocity profile associated with shear-thinning behavior (Fig. 14). The lower viscosity values near the die entrance and along the walls result from the locally higher shear rates in these regions, which enhances the shear-thinning effect.

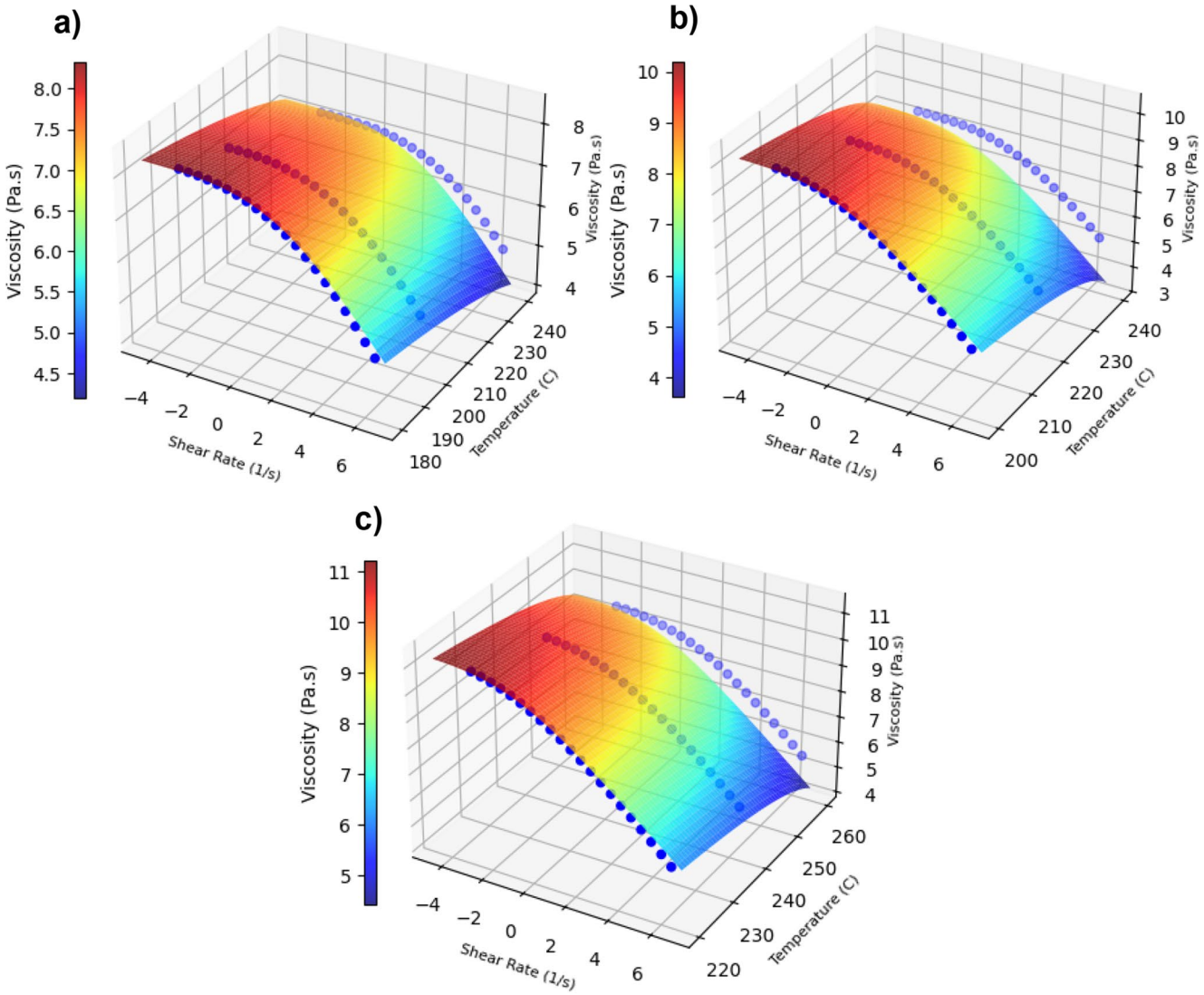

Fig. 13 Fit results of the MVI viscosity model on independent validation datasets: (a) Polypropylene (PP) (b) Polystyrene (PS) (c) Acrylonitrile-Butadiene-Styrene (ABS)

Table 5 Quantitative performance of MVI model with different materials

Material	R^2	BIC	RMSSR
PP	0.990	624.5	1.00629
PS	0.957	938.1	1.00416
ABS	0.977	1005.3	1.00456

Table 6 Needed iterations for fitting models

Material	Carreau-Arrhenius	MVI
PP	155	74
PS	341	55
ABS	367	43

Over a 20-second simulation period, runs using the MVI model required about 1.5–2.5% less computational time and exhibited more stable convergence than corresponding simulations with the Carreau-Arrhenius model under identical conditions. Separate micro-benchmarks of the constitutive laws showed that a single evaluation of the MVI expression is roughly four times faster than the Carreau-Arrhenius formulation, reflecting its simplified algebraic structure. In the CFD simulations, this translated into slightly reduced overall computational effort. This relative gain is expected to become more significant in large-scale simulations, such as extruder flows with multiple length scales, where viscosity must be evaluated millions of times.

Table 7 Pressure drop results comparison in 80 °C and 1.78 *mm/s*

Experiment	Pressure Drop (bar)
	168.9
Carreau-Arrhenius	153.5
MVI	169.9

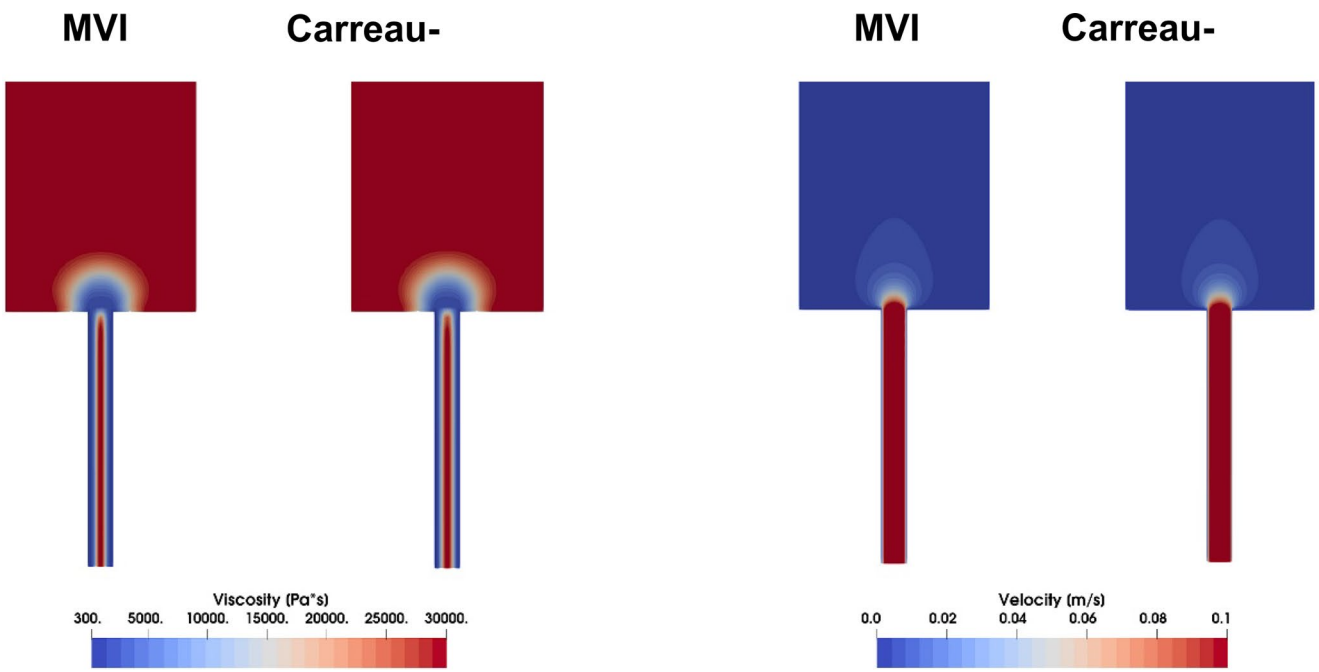

Fig. 14 Viscosity (left) and velocity (right) contour plots for both Carreau-Arrhenius and the MVI viscosity model

Conclusion

The viscosity of a shear-thinning elastomer compound was analyzed as a function of shear rate and temperature. Given the numerous applications of polymer solutions, accurately modeling their viscosity is crucial to ensuring optimal performance in various engineering and industrial applications. Classical shear rate-dependent viscosity models, such as the Power Law, Cross, and Carreau models, cannot inherently capture the effect of temperature on viscosity. To address this limitation, models such as Arrhenius, WLF, and VTF are combined with them. However, the resulting models involve complex mathematical formulations that can be computationally expensive, particularly in numerical simulations of complex geometries.

The proposed Multi-Variable Implicit (MVI) viscosity model demonstrated significant accuracy while offering a simpler five-parameter mathematical structure, making it a more efficient alternative to classical viscosity models. This advantage is particularly beneficial for numerical simulation applications, such as Computational Fluid Dynamics (CFD) frameworks, by reducing computational effort without compromising accuracy. Capillary-flow CFD simulations demonstrate that the MVI model reproduces the measured pressure-flow behavior of the elastomer with accuracy comparable to, and in this case slightly better than, the Carreau-Arrhenius model, while reducing both the computational cost of the viscosity evaluations and the number of iterations required during parameter fitting. Independent validation on three additional thermoplastics shows that the same functional form, with re-identified coefficients, can represent a broad range of polymer types and processing conditions with high accuracy.

Additionally, the MVI model effectively captures zero-shear viscosity by introducing a Newtonian plateau, which enhances numerical stability and ensures physically meaningful results across a wide range of shear rates. The combination of simplicity and high predictive accuracy makes the proposed model a valuable tool for practical applications in polymer processing and other fluid flow scenarios.

It should be noted that the current formulation of the MVI model was not trained to capture the second Newtonian plateau at high shear rates, as it does not introduce any numerical instability. However, this behavior can be captured by incorporating a suitable limiter into the model formulation. Despite this, the model's simplicity and inherent predictive capabilities suggest promising potential for future development, allowing it to incorporate high shear rate Newtonian plateau while maintaining its computational efficiency.

Acknowledgements The authors acknowledge financial support through the COMET Centre CHASE, funded within the COMET−Competence Centers for Excellent Technologies programme by the BMK, the BMDW and the Federal Provinces of Upper Austria and Vienna. The COMET programme is managed by the Austrian Research Promotion Agency (FFG). Special thanks are extended to Karin Wieland for her valuable support and contributions. Her insights and encouragement were greatly appreciated throughout this work. The authors acknowledge TU Wien Bibliothek for financial support through its Open Access Funding Programme.

Funding Open access funding provided by TU Wien (TUW).

Data availability The data are available on request.

Declarations

Competing interests The authors declare that they have no competing interests.

Confl icts of interest The authors report no confl ict of interest.

References

Angelis D, Sofos F, Karakasidis TE (2023) Artificial intelligence in physical sciences: symbolic regression trends and perspectives. Arch Comput Methods Eng 30:3845–3865

Aşıkgil B (2017) Robust nonlinear least squares approaches for evaluating OVA-mediated bleaching reactions: an experimental comparative study. Gazi University Journal of Science 30:599–608

Ayoub MA, Raja DM, Al-Marhoun MA (2007) Evaluation of Below Bubble Point Viscosity Correlations & Construction of a New Neural Network Model. In: Asia Pacific Oil and Gas Conference and Exhibition. SPE, Jakarta, Indonesia, p SPE-108439-MS

Azeez S, Bertola V (2021) Lubrication of journal bearings by shear thinning lubricants using different constitutive models. Proc Institution Mech Eng Part J: J Eng Tribology 235(6):1203–1210. https://doi.org/10.1177/1350650120950521

Bagley EB (1957) End corrections in the capillary flow of polyethylene. J Appl Phys 28(5):624–627. https://doi.org/10.1063/1.1722814

Bair S (2018) Generalized Newtonian viscosity functions for hydrodynamic lubrication. Tribol Int 117:15–23. https://doi.org/10.1016/j.triboint.2017.08.014

Brindle A (1980) Genetic algorithms for function optimization. University of Alberta Library

Budelmann D, Schmidt C, Meiners D (2020) Prepreg tack: a review of mechanisms, measurement, and manufacturing implication. Polym Compos 41(9):3440–3458. https://doi.org/10.1002/pc.25642

Carreau PJ (1972) Rheological equations from molecular network theories. Trans Soc Rheol 16(1):99–127. https://doi.org/10.1122/1.549276

Cassar DR (2021) ViscNet: neural network for predicting the fragility index and the temperature-dependency of viscosity. Acta Mater. https://doi.org/10.1016/j.actamat.2020.116602

Chapman N, Chapman M, Euler WB (2021) Modeling of poly(methylmethacrylate) viscous thin films by spin-coating. Coatings 11(2):198. https://doi.org/10.3390/coatings11020198

Chhabra RP, Richardson JF (2008) Non-Newtonian Fluid Behaviour. Non-Newtonian Flow and Applied Rheology. Elsevier, pp 1–55

Cranmer M (2023) Interpretable Machine Learning for Science with PySR and SymbolicRegression.jl

Dolz M, Delegido J, Casanovas A, Hern a-J (2005) A Low-. Cost Experiment on Newtonian and Non-Newtonian Fluids

Dominic P, Leahy D, Willis M (2010) GPTIPS:An Open Source Genetic Programming Toolbox For Multigene Symbolic Regression. Lecture Notes in Engineering and Computer Science 2180

Duretek I, Schuschnigg S, Gooneie A, Langecker GR, Holzer C (2015) Rheological properties of wood polymer composites and their role in extrusion. J Phys Conf Ser 602:012014. https://doi.org/10.1088/1742-6596/602/1/012014

Elsharkwy AM, Gharbi RBC (2001) Comparing classical and neural regression techniques in modeling crude oil viscosity. Adv Eng Softw 32(3):215–224. https://doi.org/10.1016/S0965-9978(00)00083-1

Fayed HE, Sheikh NA, Iliev O (2016) On laminar flow of non-Newtonian fluids in porous media. Transp Porous Media 111(1):253–264. https://doi.org/10.1007/s11242-015-0592-8

Ferri D, Perolo A, Nodari M, Buonerba C (2017) Cross-WLF parameters to predict rheological properties of polylactic acid

Fog A, others (2011) Instruction tables: Lists of instruction latencies, throughputs and micro-operation breakdowns for Intel, AMD and VIA CPUs. Cph Univ Coll Eng 93:110

Gholamy A, Kreinovich V, Kosheleva O (2018) Why 70/30 or 80/20 Relation Between Training and Testing Sets. A Pedagogical Explanation

Gołdasz J, Sapiński B (2015) CFD Study of the Flow of MR Fluids. Insight into Magnetorheological Shock Absorbers. Springer International Publishing, Cham, pp 117–130

Goldberg DE, Deb K (1991) A comparative analysis of selection schemes used in genetic algorithms. In: Foundations of Genetic Algorithms. Elsevier, pp 69–93

Hajizadeh Y (2007) Intelligent Prediction of Reservoir Fluid Viscosity. In: Production and Operations Symposium. SPE, Oklahoma City, Oklahoma, U.S.A., p SPE-106764-MS

Hassan M, Faisal A, Javid K, Khan S, Ahmad A, Khan R (2022) The impact of different arrangements of molecular chains in terms oflow and high shear rate's viscosities on heat and mass flow of nonnewtonianshear thinning fluids. CCHTS 25(7):1115–1126. https://doi.org/10.2174/1386207324666210719111909

Hopmann C, Michaeli W (2016) Extrusion Dies for Plastics and Rubber: Design and Engineering Computations, 4th edn. Carl Hanser Verlag GmbH & Co. KG, München

Hou J, Chen X, Wu T, Kuhl E, Wang X (2024) Automated data-driven discovery of material models based on symbolic regression: a case study on the human brain cortex. Acta Biomater 188:276–296. https://doi.org/10.1016/j.actbio.2024.09.005

Juster HR, Distlbacher T, Steinbichler G (2014) Viscosity analysis of a polymer-based drug delivery system using open-source CFD methods and high-pressure capillary rheometry. Int Polym Process 29(5):570–578. https://doi.org/10.3139/217.2892

Karimi S, Dabagh M, Vasava P, Dadvar M, Dabir B, Jalali P (2014) Effect of rheological models on the hemodynamics within human aorta: CFD study on CT image-based geometry. J Non-Newton Fluid Mech 207:42–52. https://doi.org/10.1016/j.jnnfm.2014.03.007

Kim S-Y, Park S-H (2018) Identification of Cross-WLF Viscosity Model Parameters Using Optimization Technique 최적화기법을 이용한 Cross-WLF점도 모델 계수 추정. Journal of the Korea Academia-Industrial cooperation Society 19(4):623–632. https://doi.org/10.5762/KAIS.2018.19.4.623

Koza JR (1994) Genetic programming as a means for programming computers by natural selection. Stat Comput 4:87–112

Kukla C, Duretek I, Gonzalez-Gutierrez J, Holzer C (2017) Rheology of PIM feedstocks. Met Powder Rep 72(1):39–44. https://doi.org/10.1016/j.mprp.2016.03.003

Laun HM (2004) Capillary rheometry for polymer melts revisited. Rheol Acta 43(5):509–528. https://doi.org/10.1007/s00397-004-0387-2

Li D, Zhang X, Kang Q (2023) Machine learning estimation of crude oil viscosity as function of API, temperature, and oil composition: model optimization and design space. PLoS One. https://doi.org/10.1371/journal.pone.0282084

Liu L, Liu S, Yang Y, Guo X, Sun J (2024) A generalized grey model with symbolic regression algorithm and its application in predicting aircraft remaining useful life. Eng Appl Artif Intell. https://doi.org/10.1016/j.engappai.2024.108986

Mallamace D, Mensitieri G, Salzano De Luna M, Mallamace F (2024) The time–temperature superposition of polymeric rubber gels treated by means of the mode-coupling theory. Gels 10(5):313. https://doi.org/10.3390/gels10050313

Marschik C, Roland W, Löw-Baselli B, Miethlinger J (2017) A heuristic method for modeling three-dimensional non-Newtonian flows of polymer melts in single-screw extruders. J Nonnewton Fluid Mech 248:27–39

McConaghy T (2011) FFX: Fast, Scalable, Deterministic Symbolic Regression Technology. pp 235–260

Mewis J, Wagner NJ (2011) Colloidal Suspension Rheology, 1st edn. Cambridge University Press

Newville M, Stensitzki T, Allen DB, Ingargiola A (2014) LMFIT: non-linear least-square minimization and curve-fitting for python

Popova VA, Surovtsev NV (2014) Transition from Arrhenius to non-Arrhenius temperature dependence of structural relaxation time in glass-forming liquids: continuous versus discontinuous scenario. Phys Rev E. https://doi.org/10.1103/PhysRevE.90.032308

Rabhi F, De Larochelambert T, Barriere T, Ramel D, Cousin T, Sahli M (2024) Experimentation, identification, and simulation of polymer swelling at extrusion die outlets. Polym Eng Sci 64(8):3817–3833. https://doi.org/10.1002/pen.26814

Rabinowitsch B (1929) Über die Viskosität und Elastizität von Solen. Zeitschrift für Physikalische Chemie 145A(1):1–26. https://doi.org/10.1515/zpch-1929-14502

Radwan M, Schneider S, Müller TE, Frerich S (2024) Understanding the dynamics of polymer extrusion: simulation of thermoplastics processing with planetary roller extruders. Heliyon 10(7):e28729. https://doi.org/10.1016/j.heliyon.2024.e28729

Recondo MP, Elizalde BE, Buera MP (2006) Modeling temperature dependence of honey viscosity and of related supersaturated model carbohydrate systems. J Food Eng 77(1):126–134. https://doi.org/10.1016/j.jfoodeng.2005.06.054

Rudolph NM, Agudelo AC, Granada JC, Park HE, Osswald TA (2016) WLF model for the pressure dependence of zero shear viscosity of polycarbonate. Rheol Acta 55(8):673–681. https://doi.org/10.1007/s00397-016-0945-4

Ruschak KJ, Weinstein SJ (2014) A local power-law approximation to a smooth viscosity curve with application to flow in conduits and coating dies. Polym Eng Sci 54(10):2301–2309. https://doi.org/10.1002/pen.23782

Saadat M, Mahmoudabadbozchelou M, Jamali S (2022) Data-driven selection of constitutive models via rheology-informed neural networks (RhINNs). Rheol Acta 61(10):721–732. https://doi.org/10.1007/s00397-022-01357-w

Salehi MS, Esfidani MT, Afshin H, Firoozabadi B (2018) Experimental investigation and comparison of Newtonian and non-Newtonian shear-thinning drop formation. Exp Therm Fluid Sci 94:148–158. https://doi.org/10.1016/j.expthermflusci.2018.02.006

Schmidt M, Lipson H (2009) Distilling free-form natural laws from experimental data. Science 324(5923):81–85. https://doi.org/10.1126/science.1165893

Syrjälä S, Aho J (2012) Capillary rheometry of polymer melts - simulation and experiment. Korea Aust Rheol J 24(3):241–247. https://doi.org/10.1007/s13367-012-0029-7

Tanguy PA, Choplin L, Hurez P (1988) Compensation effects in viscosity-temperature dependence of polymer melts. Polym Eng Sci 28(8):529–533. https://doi.org/10.1002/pen.760280807

Tanmay VS, Patne R, Shankar V (2018) Stability of plane Couette flow of Carreau fluids past a deformable solid at arbitrary Reynolds numbers. Phys Fluids. https://doi.org/10.1063/1.5041771

Udrescu S-M, Tegmark M (2020) AI Feynman: A physics-inspired method for symbolic regression

Vlachopoulos J, Polychronopoulos N (2011) Basic Concepts in Polymer Melt Rheology and Their Importance in Processing. In: Kontopoulou M (ed) Applied Polymer Rheology, 1st edn. Wiley, pp 1–27

Wrobel M (2020) On the application of simplified rheological models of fluid in the hydraulic fracture problems. Int J Eng Sci. https://doi.org/10.1016/j.ijengsci.2020.103275

Yasuda K (2005) Investigation of the analogies between viscometric and linear viscoelastic properties of polystyrene fluids /